Retrieval of Cloud Cover Parameters from Multispectral Satellite Images

ALBERT ARKING

Goddard Laboratory for Atmospheres Sciences, NASA/Goddard Space Flight Center, Greenbelt, MD 20771

JEFFREY D. CHILDS

Systems and Applied Sciences Corporation, Vienna, VA 22180

(Manuscript received 6 September 1983, in final form 11 December 1984)

ABSTRACT

A technique is described for extracting cloud cover parameters from multispectral satellite radiometric measurements. Utilizing three channels (visible, 3.7 μm and 11 μm) from the AVHRR (Advanced Very High Resolution Radiometer) on NOAA polar orbiting satellites, it is shown that one can retrieve four parameters for each pixel: cloud fraction within the FOV, optical thickness, cloud-top temperature and a microphysical model parameter. The last parameter is an index representing the properties of the cloud particle (e.g., size, shape, thermodynamic phase, etc.) and is determined primarily by the radiance at 3.7 μm. The other three parameters are extracted from the visible and 11 μm infrared radiances, utilizing the information contained in the two-dimensional scatter plot of the measured radiances. The solution is essentially one in which the distributions of optical thickness and cloud-top temperature are maximally clustered for each region, with cloud fraction for each pixel adjusted to achieve maximal clustering.

1. Introduction

Ever since the first image of the Earth was transmitted from a free-flying satellite (TIROS-1) in 1960, there has been a growing interest in utilization of the space platform to collect data on cloud cover and in the development of a cloud climatology data set. The major obstacles have always been 1) establishing a relationship between cloud amount and the brightness distribution within the image, and 2) data volume. The first successful attempt to extract cloud amounts from satellite imagery was carried out by Arking (1964). In that effort the video signal from the satellite image was digitized and processed by a computer. Cloud fractions were determined by using thresholds selected by a 'man-in-the-loop" who used context and meteorological judgement. A parallel effort, but utilizing manual processing, was conducted at NOAA by Clapp (1964), who utilized a planimeter to convert hand-drawn nephanalyses, based upon the perceived cloud pattern in a series of satellite images, into areas and cloud fractions. There was substantial agreement in the results of the two efforts.

With the advent of calibrated, multichannel imagery and the great increase in computer power, it has now become possible to utilize more objective techniques—not only to extract cloud amount but to obtain some of the other cloud parameters at the same time. In 1972, the Scanning Radiometer (SR) on the polar orbiting operational meteorological satellites began providing on a daily basis a near-complete mosaic of the Earth, once per 12 hours, in the visible and thermal infrared regions of the spectrum. Rossow *et al.* (1983) used the data from those channels to derive cloud amount, optical thickness, and cloud-top temperature in a pilot program to develop a cloud climatology based upon SR imagery.

A new generation of polar orbiting meteorological satellites was initiated in October 1978 with the launch of the TIROS-N satellite. The SR was replaced with the Advanced Very High Resolution Radiometer (AVHRR), which yields images in four channels (0.73, 0.90, 3.7 and 11 μm). The additional channels provide a potential for extracting more information than can be extracted from two channels. (Beginning with the second satellite of the TIROS-N series, designated NOAA 6, the wavelength of the first channel was reduced to 0.63 μm; on the NOAA 7 satellite, the third in the TIROS-N series, there is a fifth channel at 12.0 μm.)

With the growing interest in developing a cloud climatology, there are now a number of techniques for extracting cloud cover parameters from the satellite measurements. They can generally be divided into two classes: 1) those using radiative transfer calculations combined with a *threshold* test to detect cloudy pixels and 2) those based upon identification of *clusters* in the multidimensional radiance space formed by one or more channels.

The threshold technique treats each pixel independently and uses the simplifying assumption that the field of view (FOV) is either completely clear or

completely cloudy. In other words, if f is the fraction of the FOV covered by clouds, f is allowed only the values $f = 0$ or 1, depending upon the radiance in one or more channels. The independence of the pixels implies that the number of pieces of information extracted cannot exceed the number of channels. Thus, if one were utilizing two channels—e.g., visible and infrared—one might expect to determine the optical thickness δ and cloud-top temperature T_c. This is essentially the method utilized by Rossow *et al.* (1983).

Because the threshold method treats each pixel independently, the processing of the data is fairly straightforward and free from the problems associated with cognitive-type algorithms. Furthermore, it allows for strict application of the equations of radiative transfer, which directly relate the radiative properties of the cloud to the radiances measured in each channel. The disadvantages of the threshold approach all stem from the fairly high likelihood that f is neither 0 nor 1, but somewhere in between, as demonstrated by Coakley and Bretherton (1982). If the threshold were chosen to balance out the errors in determining mean cloud cover fractions for one cloud type, then biases would appear for other cloud types. Even more serious is the problem in determining the other parameters, such as δ and T_c. The distributions of these parameters would be biased towards the center because when only part of the FOV is filled, thick and cold clouds would appear less thick and warmer, and thin and warm clouds would fall below the threshold and be counted as clear. The most serious difficulty with the threshold method is the dependence of the results upon the resolution (i.e., pixel size): the larger the pixel, the less accurate the results because the greater the likelihood that f is neither 0 nor 1.

The cluster approach is specifically aimed at dealing with the problem of clouds filling only part of the FOV. The idea behind this approach is that if the cloud masses are generally larger than the pixels and the cloud and surface radiances are fairly uniform, then those pixels for which $f = 0$ or 1 will tend to cluster in the multidimensional scatter plot of the measurements in each channel, while pixels with $0 < f < 1$ will spread out. When more than one cloud type or surface appears within the region under analysis, then there will appear multiple clusters. Debois *et al.* (1982) describes one method for detecting such clusters in two dimensions. It is also possible to work with one-dimensional clusters; an example is the method of Coakley and Bretherton (1982), which is applied to the infrared channel alone.

Once clusters are identified, the determination of f and other radiative parameters depends upon the channels available and the technique used. Coakley and Bretherton (1982) determine two parameters: the cloud fraction f and an effective radiative temperature of the cloud, which would be the cloudtop temperature T_c if the cloud were optically thick. Debois *et al.* (1982) determine T_c using two infrared channels, as described by Szejwach (1982).

In this study we combine the best features of the two approaches, utilizing the equations of radiative transfer, as in the threshold method, and the identification of clusters in the two-dimensional scatter plot of the radiances in the visible and 11 μm infrared channels. Information from a third channel, at 3.7 μm, is used to determine the microphysical model of the cloud particles.

2. Theory

Under certain simplifying assumptions the radiances measured in the AVHRR channels depend upon four cloud parameters:

- f cloud cover fraction within FOV,
- δ optical thickness of cloud layer at a reference wavelength,
- T_c cloud-top temperature,
- m microphysical model (MPM) of cloud particle.

In limiting the retrieval to these four parameters, it is assumed that within the FOV there is only one cloud type, with vertically and horizontally uniform temperature and optical properties. In addition, there are surface parameters (viz., surface temperature and reflectivity) which are also assumed to be uniform.

The microphysical model parameter m is simply an index that represents the distribution of size, shape and index of refraction of the cloud particle. In this study we have considered only spherical water droplets and ice particles, with a size distribution given by:

$$\frac{dN(r)}{dr} \propto r^6 e^{-6r/r_0},$$

where $N(r)$ is the number of particles per unit volume with radii smaller than r, and r_0 is the mode radius. For this distribution the mean radius is 7/6 r_0 and the effective radius is 3/2 r_0. Six possible MPMs are considered in this study, representing water droplets and spherical ice particles of various sizes. They are shown in Table 1 along with their optical properties at the wavelengths corresponding to the three channels that will be used in this study; they were computed using Mie theory (King, 1983).

The optical thickness of the cloud layer is defined by $\delta = n\sigma\Delta z$, where n is the particle density in the cloud, σ the particle extinction coefficient, and Δz the geometrical thickness of the layer. The optical thickness depends upon wavelength and MPM, as shown in Table 1, but here δ refers exclusively to a reference wavelength of 0.73 μm, the central wavelength of the visible channel of the TIROS-N AVHRR.

The cloud-top temperature represents the physical temperature of the cloud layer if it were vertically

TABLE 1. Microphysical models and their optical parameters.

MPM index	Mode radius r_0 (μm)	Particle phase	TIROS-N channel (μm)	Extinction coefficient σ (cm^2/particle)	Particle albedo	Asymmetry factor
			0.73	1.68*E*-6	1.000	0.845
1	4	liquid	3.7	2.01*E*-6	0.937	0.753
			11	0.88*E*-6	0.383	0.856
			0.73	1.68*E*-6	1.000	0.863
2	4	ice	3.7	1.98*E*-6	0.884	0.751
			11	1.16*E*-6	0.305	0.843
			0.73	6.55*E*-6	1.000	0.863
3	8	liquid	3.7	7.18*E*-6	0.878	0.820
			11	5.93*E*-6	0.494	0.938
			0.73	6.55*E*-6	1.000	0.871
4	8	ice	3.7	7.17*E*-6	0.799	0.837
			11	5.97*E*-6	0.411	0.927
			0.73	2.57*E*-5	1.000	0.873
5	16	liquid	3.7	2.73*E*-5	0.801	0.873
			11	2.83*E*-5	0.514	0.966
			0.73	1.02*E*-3	1.000	0.887
6	32	ice	3.7	1.06*E*-3	0.606	0.936
			11	1.05*E*-3	0.503	0.967

uniform. (To the extent that temperature changes with depth, T_c represents a weighted mean over the penetrable portion of the cloud.) For optically thin clouds, or where $f < 1$, there can be considerable differences between T_c and the measured brightness temperature T_{11}.

In principle, the optical effects of the atmosphere could be taken into account. It would require *a priori* information on the state of the atmosphere, involving a large number of variables and a more complicated set of equations. However, the net effect on the final results is expected to be small because i) the channels are in relatively clear portions of the atmospheric spectrum, and ii) the surface optical properties are determined by the same channels that are used to infer the cloud optical properties. The second condition implies that what we call the "surface" is the actual surface plus the overlying atmosphere. Since the "surface" is placed radiatively below the cloud base level, it is only the atmosphere *above* the cloud base level that is neglected by our simplifying assumptions.

To assess the effects of the atmosphere above cloud base level, line-by-line calculations of upward and downward fluxes at various levels in a midlatitude summer atmosphere (A. Arking and W. L. Ridgway, unpublished paper presented at the Workshop on the Intercomparison of Radiation Codes for Climate Models, Frascati, Italy, August, 1984) were utilized. They show that the 11 μm brightness temperature (based upon outgoing flux at the top of the atmosphere, integrated over 2π steradians, between 850 and 950 cm^{-1}, where most of the radiation is concentrated) is affected by the atmosphere above 500 mb by 0.3°C, above 700 mb by 1.1°C, and above 850 mb by 2.4°C. At 3.7 μm, it is even smaller. Assuming a lapse rate of 5.5°C km^{-1}, the effect on the determined height of the cloud is generally less than 0.5 km for optically thick clouds that nearly fill the FOV. The visible channel, which extends from 0.55 to 0.90 μm on TIROS-N (0.58 to 0.68 μm on subsequent satellites), is affected by absorption due to oxygen at 0.76 μm and water vapor at 0.73 and 0.81 μm, but because of the width of the spectral region and narrowness of the bands the effect is small.

To obtain the four cloud parameters the information from three channels will be used:

R_v reflectance in the visible channel,
T_{11} 11 μm brightness temperature,
I_3 3.7 μm radiance.

Using a doubling method (King, 1983), radiative transfer calculations were performed to determine the reflection and transmission properties of the cloud layer as a function of optical thickness for each microphysical model. An example, at a wavelength of 3.7 μm, is shown in Fig. 1. At this wavelength the reflectance is highly dependent upon particle size and phase, providing the information needed to determine the microphysical model. The visible channel, on the other hand, is sensitive primarily to optical thickness, while the 11 μm channel is sensitive primarily to the cloud-top temperature. Thus, given f, the measurements in the three channels are sufficient to determine δ, T_c and m in each pixel. However, since f is to be treated as an unknown, it is necessary to find an

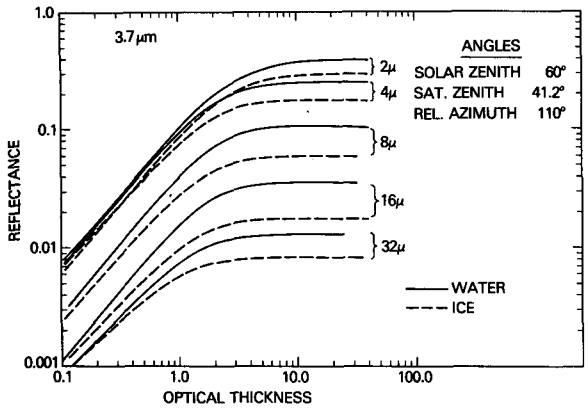

FIG. 1. Theoretical calculations of the reflectance at 3.7 μm versus optical thickness for plane parallel clouds with various particle mode radii and thermodyamic phase; the size distribution is given in the text.

additional constraint. As shown below, this constraint is based upon the relationships of the points in an R_v–T_{11} scatter diagram.

The algorithm for determining δ, T_c and m, given f, requires a set of equations that relate the scene parameters within each FOV to the radiances in the three channels. In addition to the cloud transmission and reflection functions, one requires the surface optical properties, which include its reflectivity in the visible channel and its radiance in the 3.7 and 11 μm channels. (The reflectance at 11 μm is assumed to be 0.) They are retrieved from pixels that are determined to be cloud-free in a manner to be described in the next section.

The equations that relate the cloud transmission and reflection functions, the cloud fraction f, and the aforementioned surface properties to the measured radiance in each channel are straightforward. They are exhibited and explained in the Appendix. The equations include the transmission, reflection and absorption of solar radiation by the cloud layer in the visible and 3.7 μm channels, and emission, absorption, transmission and reflection of thermal radiation by the cloud layer in the 3.7 and 11 μm channels. The effects of multiple reflections between the surface and the cloud base are included.

To understand the following algorithm description, it is convenient to consider the set of equations that transform the parameters f, δ, T_c and m into radiance in each of the three channels [Eq. (A7) in the Appendix] as an operator denoted by

$$(R_v, I_3, T_{11}) = \mathcal{W} \cdot (f, \delta, T_c, m).$$

Because the mapping from (f, δ, T_c, m) to (R_v, I_3, T_{11}) is not one to one, there is a range of values of (f, δ, T_c, m) consistent with the measured radiances. While there is no unique mathematical solution, it is possible to utilize known physical attributes of cloud cover (e.g., the tendency to form a cloud mass) to constrain the solution. The intent here is to develop an algorithm (or inverse) that yields a solution that is "most reasonable" in a statistical sense.

A subset of the operator $\mathcal{W}$ is one that, given f, m and the surface properties, transforms δ and T_c into visible reflectance and 11 μm blackbody temperature,

$$(R_v, T_{11}) = \mathcal{W}_{fm} \cdot (\delta, T_c).$$

This second operator has a unique, well-defined inverse,

$$(\delta, T_c) = \mathcal{W}_{fm}^{-1} \cdot (R_v, T_{11}),$$

and is used quite often in the algorithm. While not expressible in closed form, the inverse operation $\mathcal{W}_{fm}^{-1}$ is performed by a table look-up procedure described in the Appendix.

3. Algorithm

The algorithm for extracting the cloud parameters can be broken down into the following steps:

i) selection of cloud-free pixels and retrieval of *surface parameters;*

ii) determination of the *microphysical model* (MPM);

iii) *selection of clusters* in the R_v–T_{11} two-dimensional histogram, representing cloud-filled FOVs;

iv) application of "maximal clustering" technique to determine the values of f and the other cloud parameters.

The algorithm is applied to analysis areas large enough so that the number of pixels is sufficient to establish the statistics of the radiance distribution, but small enough so that one can make certain assumptions regarding homogeneity. Each analysis area is treated independently of its neighbors, but within each area it is assumed that the surface optical properties (which, as noted above, include the effects of the atmosphere up to cloud base level) and the MPM of the cloud are uniform. The parameters allowed to vary within the analysis area are f, δ and T_c. For the application in Section 4, the analysis areas were chosen to be 2.5° latitude by 2.5° longitude.

a. *Surface parameters*

The three surface parameters—reflectance in the visible and radiances at 3.7 and 11 μm—are determined from cloud-free pixels within the 2.5° by 2.5° analysis area. The identification of cloud-free pixels is done by finding the coordinate in R_v–T_{11} space that corresponds to lowest R_v and highest T_{11} and then looking for the nearest cluster. The criterion for the existence of a cluster is based upon relative density. To guard against regions with few or no clear pixels, a test is made on surface temperature and

albedo to make sure they are within certain limits of expectation, based upon climatology. When there are no clear pixels, the surface properties are determined from neighboring analysis areas with similar topography.

b. *Microphysical model*

The parameter m is determined by assuming $f = 1$ and making the transformation

$$[\delta(m), T_c(m)] = \mathcal{W}_{1m}^{-1} \cdot (R_v, T_{11})$$

for the six possible values of m (see Table 1). Then, $I_3(m)$ is computed by the transformation

$$[R_v, I_3(m), T_{11}] = \mathcal{W} \cdot [1, \delta(m), T_c(m), m].$$

By comparing $I_3(m)$ with the observed I_3, one determines the m of best agreement. An illustration of this procedure appears in Figs. 2 and 3. In each case data were selected from an AVHRR image and processed as above. In one case the observed 3.7 μm radiance corresponds to the computations for a 32 μm radius ice particle, the other to that for a 4 μm particle. The large ice particle is associated with

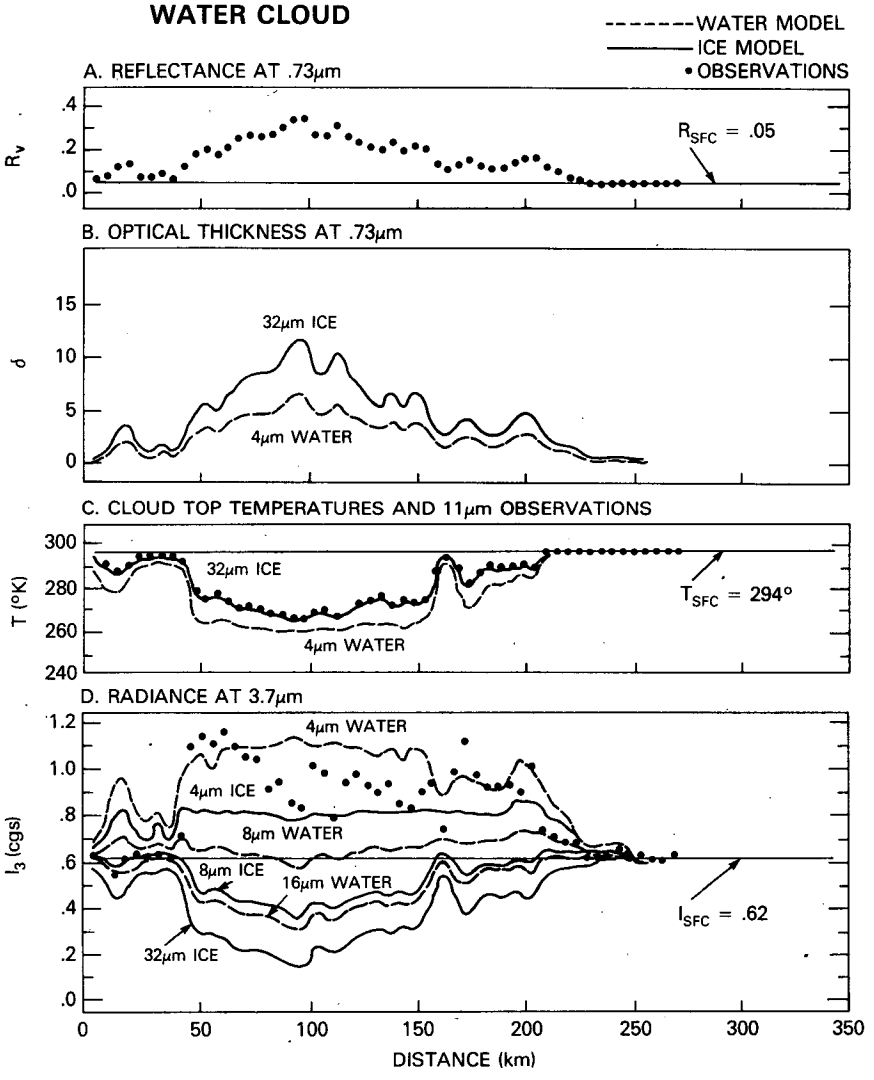

FIG. 2. Observed and derived quantities along a scan line of a NOAA 7 AVHRR image. (a) Reflectance in the visible channel. (b) Calculated optical thickness that matches the measured reflectance, shown for two of the microphysical models (MPM). (c) Calculated cloud-top temperatures T_c (dashed and solid curves) that correspond to the observed 11 μm brightness temperature T_{11} (filled circles); the differences between T_{11} and T_c are due to the nonblackbody nature of clouds, especially when thin. (d) Calculated radiance at 3.7 μm, based upon the derived δ and T_c for 6 MPMs (dashed and solid curves) compared with observed radiances (filled circles).

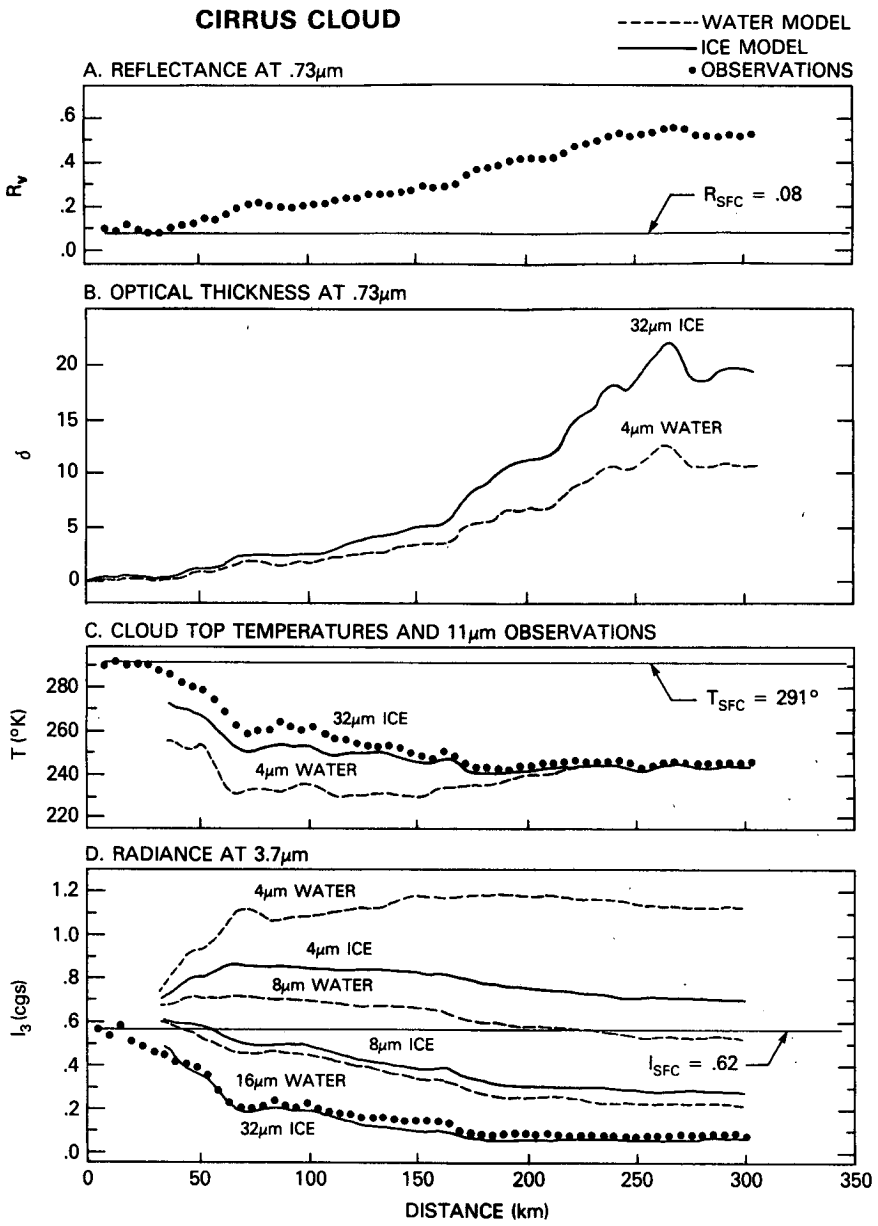

FIG. 3. As in Fig. 2 except the scan is over a cirrus cloud that appears in another part of the same image.

cirrus, and the small particle is associated with a water cloud because of the relatively high cloud-top temperature and the likelihood that when particles freeze they quickly grow.

It is clear in Figs. 2 and 3 that as the optical thickness approaches zero the values of $I_3(m)$ for different m merge towards the surface value, and the determination of m becomes ambiguous. It is likewise as f approaches zero. Now the assumption that $f = 1$, when f is actually <1, would lead to an underestimate of δ and an overestimate of T_c, thus bringing $I_3(m)$ closer to the surface value for all m, which is qualitatively similar to the effect of reducing f. In any event, the determination of m is heavily influenced by pixels where the $I_3(m)$ are more widely separated, which correspond to large δ and f close to 1. It is unlikely, therefore, that the $f = 1$ assumption will adversely affect the determination of m.

It is important to note from Figs. 2 and 3 that the retrieved parameters δ and T_c can depend significantly on the MPM. Without the knowledge gained from the 3.7 μm channel, there would be a range of

uncertainty of 10–20 K in T_c and a factor of 2 in δ, because the extreme models, 4 μm water and 32 μm ice, differ by that extent.

c. *Selection of clusters*

Plotting R_v versus T_{11} for the pixels in an analysis area yields a scatter diagram. (An example appears at the top of Fig. 4; it is from a $^1/_{16}$ portion of a 2.5° × 2.5° analysis area that was divided 4 × 4, and the surface point corresponds to that for the entire area.) Points that correspond to pixels from within relatively homogeneous portions of the image—e.g., the surface or a large cloud mass—will tend to form small clusters in the diagram. Pixels composed of mixed optical characteristics—e.g., where there is fractional cloud cover—will tend to spread out, their precise position in the diagram depending upon the relative fractions of the components. An essential feature of the cloud parameter technique presented here is the recognition of clusters within the R_v–T_{11} diagram and the assumption that $f = 1$ for pixels that fall within the clusters. Points outside the clusters are assumed to correspond to pixels with $f \leq 1$.

The method of recognizing clusters is not of primary interest in this study. There are many such methods, but for testing the algorithm it was considered satisfactory to choose the clusters based upon manual inspection of the R_v–T_{11} scatter diagram. For programming simplicity the cluster is defined by the four corners of a quadrangle. In the example at the top of Fig. 4, there is quite clearly a cluster in the vicinity of $R_v = 0.60$ and $T_{11} = 210$ K. The second cluster is less obvious but was selected because of the slightly higher local density of points.

d. *Maximal clustering technique*

To determine the cloud parameters it is necessary to determine f for pixels outside the selected clusters. An illustration of how the transformation from (R_v, T_{11}) to (δ, T_c) depends upon f is shown in Fig. 5. The pixel with $R_v = 0.55$, $T_{11} = 260$ K maps onto the upper band, and the pixel with $R_v = 0.30$, $T_{11} = 260$ K maps onto the lower band. It is seen that the values of δ and, especially, T_c, are quite sensitive to f. Also, as f becomes smaller, there is a substantial increase in the sensitivity. Determination of the microphysical model reduces the possible solution from a band to a line, with the rightmost point on the line corresponding to $f = 1$.

The method chosen to determine f is based upon "maximal clustering" and is illustrated in Fig. 4. The top diagram shows the R_v–T_{11} scatter diagram with the selected clusters. The transformation to δ–T_c for $f = 1$ is shown in the middle diagram. (The cluster boundary in the δ–T_c diagram is determined by the transform of the four corners in the R_v–T_{11} diagram.) Each point in the δ–T_c diagram, representing a pixel, can now be considered as the endpoint of a line that generally extends upward and to the left. Moving along that line corresponds to changing f, as in Fig. 5. Now, consider the clusters in the δ–T_c diagram as attractors, and allow the points outside the clusters to move along their respective lines in such a way as to maximize the density around the selected clusters. This is accomplished by locating one point on each line which is closest, in an absolute sense, to any one of the clusters. The unit of distance along each axis is defined to be the maximum dimension of the cluster along that axis. Thus, the distance scale is not fixed; it depends upon the cluster. Once the position of the point is determined, the value of f associated with that position (again, use Fig. 5 as an example) becomes the retrieved cloud cover fraction for that pixel.

To summarize the application of the above described principle of "maximal clustering", the top diagram in Fig. 4 shows the pixels in R_v–T_{11} space and the selected clusters. The middle diagram shows the transformation to δ–T_c space for $f = 1$. Finally, the bottom diagram shows the points after reducing the values of f, for points outside the clusters, in order to bring them as close as possible to the selected clusters. The result of this procedure is a determination of f, δ and T_c for each pixel, with m having been determined earlier from the information in the 3.7 μm channel.

4. Application

In order to compare methods, the International Satellite Cloud Climatology Project selected examples of data from the AVHRR imaging radiometer on the TIROS-N polar orbiting satellite for distribution to investigators. One of the test areas is off the northeast coast of South America, extending from 7.5°S to 12.5°N, 35 to 55°W. The visible channel image is shown in Fig. 6. The results of applying the algorithm described in this study are displayed in Figs. 7 and 8. Cloud fractions are determined in 2.5° latitude by 2.5° longitude analysis areas by averaging the values of f for each pixel; pixels associated with the surface cluster are assigned $f = 0$. The cloud fractions for the test area are plotted as contours in Fig. 7. The main features are the heavy cloud cover in the southwest portion of the scene, covering most of the land area, and a line of clouds that extends off the coast and expands out over the Atlantic, in the vicinity of 3°N, 38°W.

The distribution of derived cloud properties is determined for each analysis area. Then the distributions are merged and plotted as contours in Fig. 8. The bimodal distribution of thick, high clouds ($T_c \approx 225$ K) and thick, low clouds ($T_c \approx 280$ K) is consistent with the visual interpretation of Fig. 6 and the corresponding infrared image (not shown).

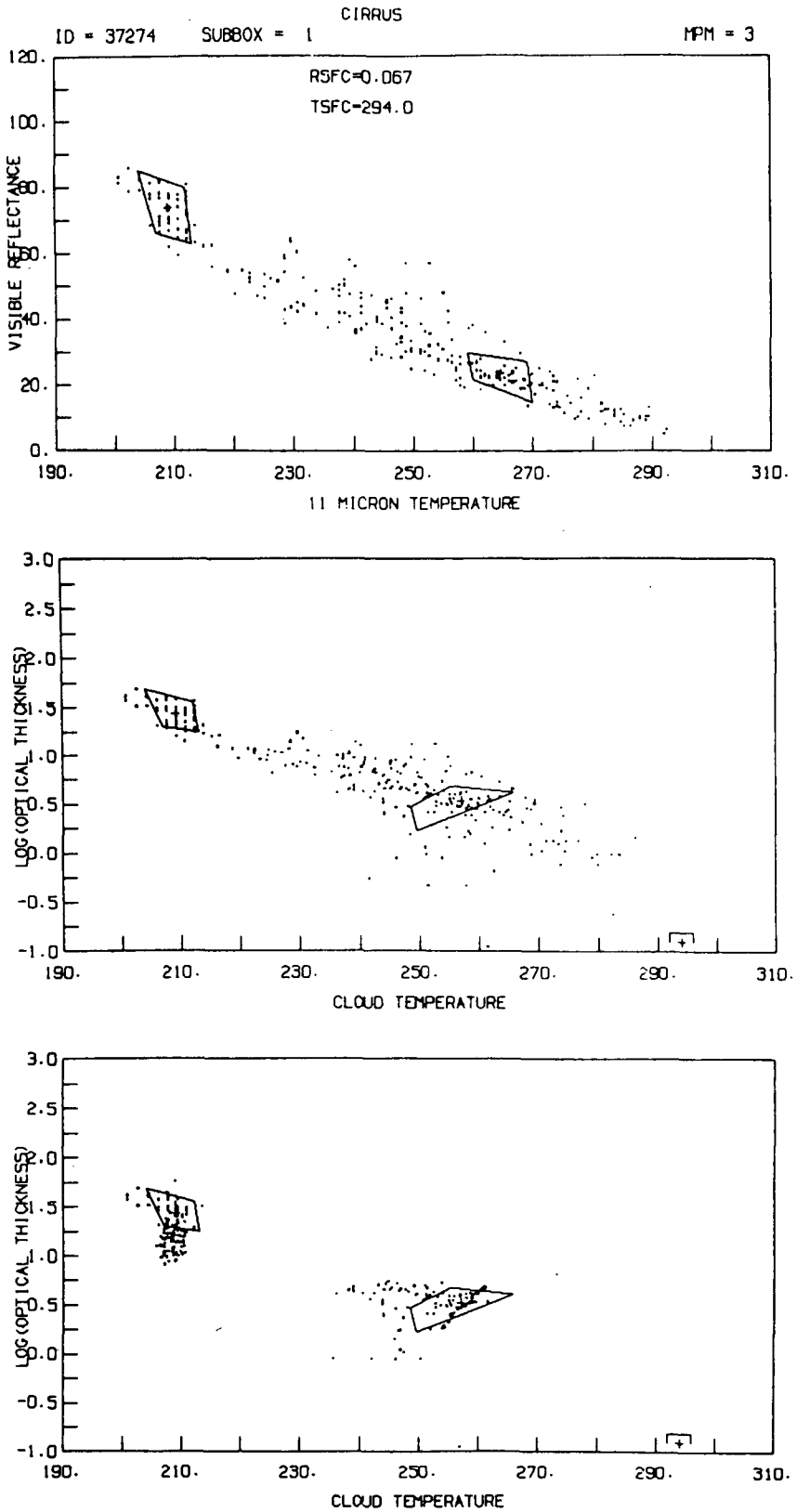

FIG. 4. The selection of clusters in the two-dimensional histogram formed by the visible and 11 μm channels (top), the transformation to the δ–T_c two-dimensional histogram assuming filled FOVs (middle), and the application of the "maximal clustering" technique (bottom) as explained in the text.

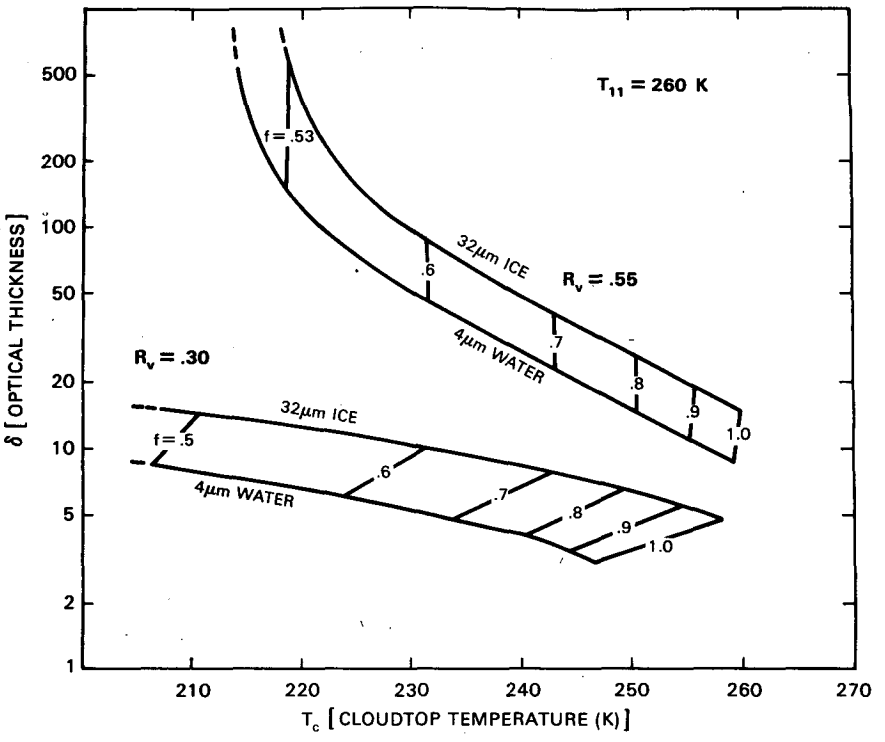

FIG. 5. Possible values of the cloud parameters δ and T_c associated with a given 11 μm brightness temperature (T_{11} = 260 K) and two values of the visible reflectance (R_v = 0.30, 0.55).

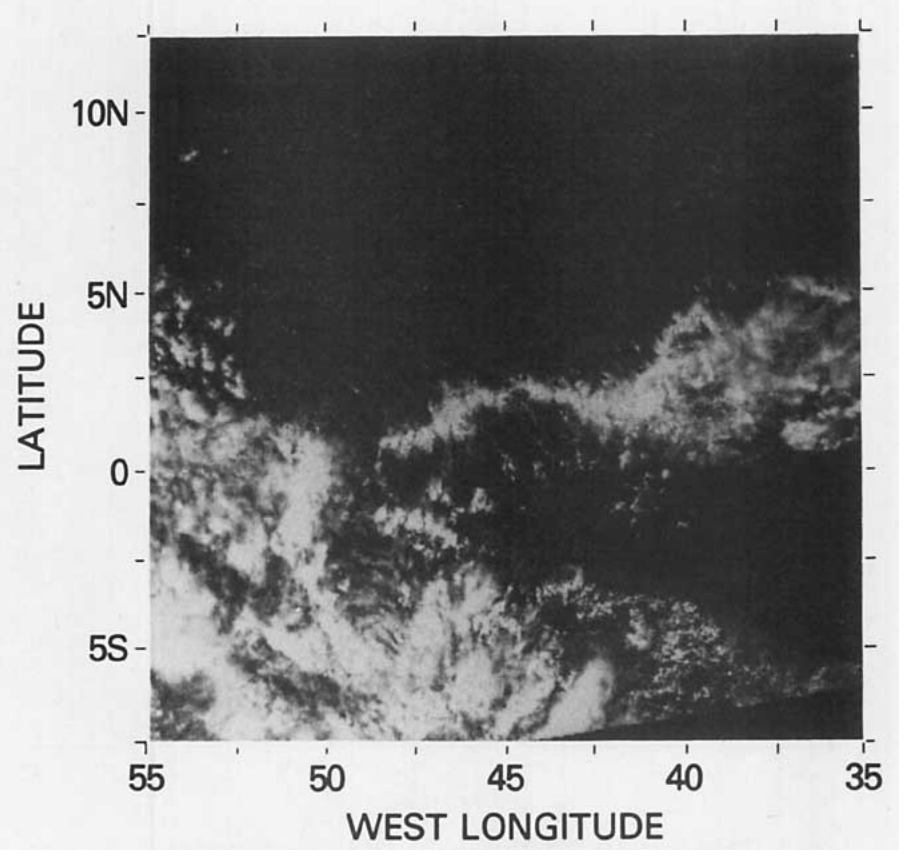

FIG. 6. Rectified image from the visible channel of the TIROS-N AVHRR at ~1800 GMT 6 February 1979, covering the area 7.5°S to 12.5°N, 35 to 55°W.

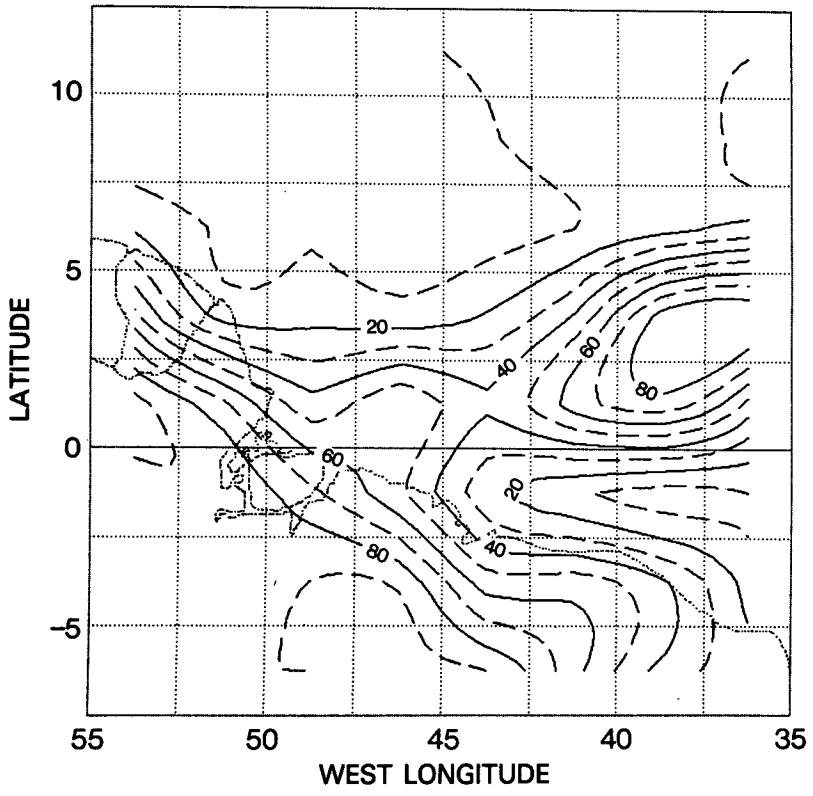

FIG. 7. Contours of cloud cover fraction for the area shown in Fig. 6, resulting from the application of the algorithm described in this study to the visible and 11 μm infrared channel measurements.

5. Summary

One approach towards retrieving cloud cover parameters has been explored and applied to a test case.

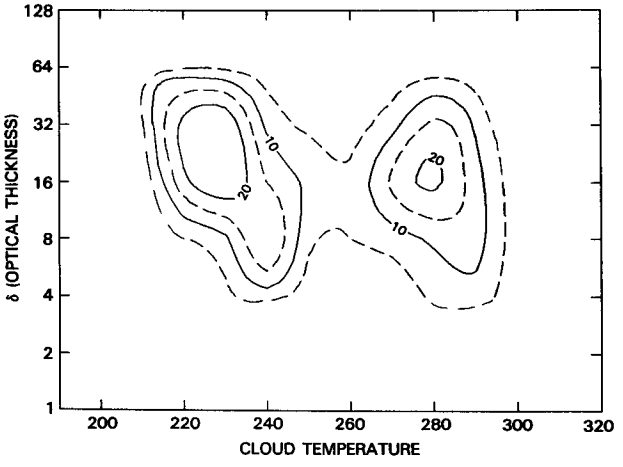

FIG. 8. Contours of the derived optical thickness and cloud-top temperature associated with the cloud cover fractions shown in Fig. 7.

The results are consistent with the visual interpretation of the visible and infrared images. The essential features of this approach are: i) it utilizes the 3.7 μm channel to determine the microphysical model that characterizes the cloud particle, and ii) it allows for the possibility of partially-filled FOVs. In the end, four parameters are retrieved (cloud cover fraction, optical thickness, cloud-top temperature, and microphysical model) from three channels (visible, 11 μm and 3.7 μm). To make it possible to retrieve four parameters from three pieces of information, it is necessary to apply constraints. This study makes use of the radiometric relationships of the pixels within a given region. The natural clustering of pixels in a scatter plot of the radiances in the visible and 11 μm channels is used to determine the cloud parameters for cloud-filled pixels. To all other pixels, the technique of *maximal clustering* is applied to determine the cloud fractions associated with those pixels that make their cloud parameters most consistent with the cloud-filled pixels. The constraint is effectively one of achieving maximum consistency in the derived cloud cover parameters, while the cloud fraction floats.

The 3.7 μm channel is used independently of the above procedure to determine the microphysical

model of best fit. The range of uncertainty, if this information were not available, could be as high as 20 K in cloudtop temperature and a factor of 2 in optical thickness.

Continuing studies will determine the sensitivity of the results to the choice of clusters and to the radiative transfer model. The stability of the results against the effects of overlapping clouds and multiple clouds within the FOV will also be tested.

APPENDIX

Reflection and Emission of Radiation from a Cloud Layer over a Lambert Surface

In order to properly interpret the multichannel radiance measurements, it is necessary to write down equations which relate the optical properties of the clouds, atmosphere and surface to the measured radiance. The relationships expressed here entail certain simplifying assumptions.

1) The radiance from any point within the field of view (FOV) can be treated as coming from a plane parallel, horizontally homogeneous medium.
2) The cloudy portion of an FOV constitutes a single layer that is vertically and horizontally homogeneous, including uniform temperature.
3) The surface in the clear portion of an FOV and below the cloud is uniform and reflects isotropically.
4) The optical effects of the atmosphere can be neglected.

The first assumption neglects the vertical extent of clouds and ignores cloud–cloud interactions. Estimates of the magnitude of these effects, the so-called "finite cloud effects," have been made by Harshvardhan and Weinman (1982) and Weinman and Harshvardhan (1982). The second, third and fourth assumptions can be made less restrictive, if necessary, provided that additional information is available on the atmosphere, cloud structure and surface optical properties. The atmospheric effects are probably not very important for the purposes of this study, inasmuch as the atmosphere is almost transparent in these channels. Also, the effect of the atmosphere below the cloud base level is to a large extent cancelled out because the cloud properties are derived by comparing the cloud radiance to the cloud-free radiance.

With the above assumptions, the optical properties of the surface are represented by the reflectance R_ν^s and of the cloud layer by the *bidirectional reflectance* $R_\nu^c(\mu_0, \mu, \phi)$ and *bidirectional transmittance* $T_\nu^c(\mu_0, \mu, \phi)$, where ν is the wavenumber representing a particular channel, μ_0 and μ are the cosines of the zenith angles of the sun and satellite, respectively, and ϕ is the azimuth angle between the solar-zenith and satellite-zenith planes. The *diffuse reflectance* of the cloud layer (i.e., the reflectance in a particular direction for isotropic incident radiation) is given by

$$\hat{R}_\nu^c(\mu) = \frac{1}{\pi}\int_0^{2\pi}\int_0^1 R_\nu^c(\mu', \mu, \phi)\mu' d\mu' d\phi, \quad \text{(A1)}$$

with a similar expression for the *diffuse transmittance* $T_\nu^c(\mu)$. The *diffuse albedo* of the cloud (i.e., the ratio of reflected flux to incident flux for an isotropic source) is given by

$$\bar{R}_\nu^c = 2\int_0^1 \hat{R}_\nu^c(\mu)\mu d\mu. \quad \text{(A2)}$$

The *flux transmittance* (i.e., ratio of transmitted flux to incident flux for an isotropic source) is given by

$$\bar{T}_\nu^c = 2\int_0^1 \hat{T}_\nu^c(\mu)\mu d\mu. \quad \text{(A3)}$$

The emissivity of the surface is

$$\epsilon_\nu^s = 1 - R_\nu^s, \quad \text{(A4)}$$

and of the cloud

$$\epsilon_\nu^c(\mu) = 1 - \hat{T}_\nu^c(\mu) - \hat{R}_\nu^c(\mu), \quad \text{(A5)}$$

with

$$\bar{\epsilon}_\nu^c = 1 - \bar{T}_\nu^c - \bar{R}_\nu^c. \quad \text{(A6)}$$

The radiance measured by the satellite can now be expressed in terms of these quantities. Assuming that a fraction f of the FOV of the radiometer is covered by cloud, the radiance is given by

$$\begin{aligned} I_\nu(\mu_0, \mu, \phi) &= (1-f)\epsilon_\nu^s B_\nu(T_s) + f\epsilon_\nu^c(\mu)B_\nu(T_c) \\ &+ f\frac{\hat{T}_\nu^c(\mu)}{1 - R_\nu^s\bar{R}_\nu^c}[\epsilon_\nu^s B_\nu(T_s) + R_\nu^s\bar{\epsilon}_\nu^c B_\nu(T_c)] \\ &+ \frac{\mu_0 S_\nu}{\pi}\left[fR_\nu^c(\mu_0, \mu, \phi) + f\frac{\hat{T}_\nu^c(\mu_0)\hat{T}_\nu^c(\mu)R_\nu^s}{1 - R_\nu^s\bar{R}_\nu^c} + (1-f)R_\nu^s\right], \quad \text{(A7)} \end{aligned}$$

where S_ν is the solar flux, T_s the surface temperature, T_c the cloud-top temperature, and $B_\nu(T)$ the Planck function. The first term in Eq. (A7) represents emitted surface radiation from the clear portion of the FOV. The second term represents direct upward emission from the cloud. The third term represents thermal radiation transmitted through the cloud, including emitted surface radiation and radiation from the cloud emitted downward and reflected by the surface. The fourth deals with solar radiation and has three parts: reflection from the cloud, reflection from the surface of radiation transmitted through the cloud, and reflection from the surface where clouds are absent. The effects of multiple reflections between the cloud and the surface are included by dividing the diffuse transmittance $\hat{T}_\nu^c(\mu)$ by $1 - R_\nu^s\bar{R}_\nu^c$.

Equation (A7) is applicable to all of the AVHRR channels. The solar term, however, is quite negligible at 11 μm, and the emission term is negligible for the visible channel. In practice, we neglect R_ν^s for the 11 μm channel, which makes it possible to determine the surface temperature directly from the measured surface radiance I_{11}^s.

The operator $\mathcal{W}$, used in the main body of the paper, transforms the cloud parameters into the measured quantities

$$(R_v, I_3, T_{11}) = \mathcal{W} \cdot (f, \delta, T_c, m). \quad \text{(A8)}$$

It is essentially the application of Eq. (A7) to each channel, noting that

$$R_v = \frac{\pi I_v}{\mu_0 S_v}$$

and T_{11} is obtained from I_{11} by inverting the Planck function,

$$T_{11} = B_{11}^{-1}(I_{11}).$$

The surface parameters T_s, R_v^s, and R_3^s, and cloud parameters f and T_c appear explicitly in Eq. (A7). The remaining two cloud parameters δ and m are implicitly included through the dependence of R_ν^c and T_ν^c on those parameters. The optical thickness δ is always defined at the wavelength of the visible channel, but the Mie calculations determine the corresponding values of the optical thickness at other wavelengths.

The $\mathcal{W}_{fm}$ operator is the $\mathcal{W}$ operator with f and m held fixed; it is essentially the application of Eq. (A7) to the visible and 11 μm channel only,

$$(R_v, T_{11}) = \mathcal{W}_{fm} \cdot (\delta, T_c). \quad \text{(A9)}$$

Its explicit form is expressed by the following equations:

$$R_v(f, \delta, m) = (1 - f)R_v^s + f\left[R_v^c(\mu_0, \mu, \phi) + \frac{\hat{T}_v^c(\mu_0)\hat{T}_v^c(\mu)R_v^s}{1 - R_v^s \bar{R}_v^c}\right], \quad \text{(A10)}$$

$$T_{11}(f, \delta, T_c, m) = B_{11}^{-1}\{(1 - f)I_{11}^s + f[\epsilon_{11}^c(\mu)B_{11}(T_c) + \hat{T}_{11}^c(\mu)I_{11}^s]\}. \quad \text{(A11)}$$

The inverse, $\mathcal{W}_{fm}^{-1}$, is applied by first determining the optical thickness δ for which Eq. (A10) agrees with the measured R_v, since f and m are fixed. It is performed by a table look-up procedure, using precalculated values of the reflection and transmission functions R_ν^c and T_ν^c. The range and quantization levels for the table are $\delta = 2^x$, where $x = -3(1)10$, and an appropriately spaced set of the angles (μ_0, μ, ϕ). Substituting the tabulated functions into Eq. (A10) yields R_v at the discrete set of δ values. Logarithmic interpolation then yields the δ for which R_v matches the observed reflectance. With δ known, one then determines the value of T_c by solving Eq. (A11),

$$T_c = B_{11}^{-1}\left\{\frac{I_{11} - I_{11}^s}{f\epsilon_{11}^c(\mu)} + \frac{I_{11}^s}{\epsilon_{11}^c(\mu)}[1 - \hat{T}_{11}^c(\mu)]\right\}. \quad \text{(A12)}$$

REFERENCES

Arking, A., 1964: Latitudinal distribution of cloud cover from TIROS III photographs. *Science,* **143,** 569–572.

Clapp, P. F., 1964: Global cloud cover for seasons using TIROS nephanalyses. *Mon. Wea. Rev.,* **92,** 495–507.

Coakley, J. A., and F. P. Bretherton, 1982: Cloud cover from high-resolution scanner data: Detecting and allowing for partially filled fields of view. *J. Geophys. Res.,* **87,** 4917–4932.

Desbois, M., G. Seze and G. Szejwach, 1982: Automatic classification of clouds on METEOSAT imagery: Application to high-level clouds. *J. Appl. Meteor.,* **21,** 401–412.

Harshvardhan, and J. A. Weinman, 1982: Infrared radiative transfer through a regular array of cuboidal clouds. *J. Atmos. Sci.,* **39,** 1853–1861.

King, M. D., 1983: Number of terms required in the Fourier expansion of the reflection function for optically thick atmospheres. *J. Quant. Spectrosc. Radiat. Transfer,* **30,** 143–161.

Rossow, W. B., E. Kinsella and L. Garder, 1983: Seasonal and global cloud variations deduced from polar orbiting satellite radiance measurements. *Proc. Fifth Conf. on Atmospheric Radiation,* Baltimore, Amer. Meteor. Soc., 195–198.

Szejwach, G., 1982: Determination of semitransparent cirrus cloud temperature from infrared radiances: Application to METEOSAT. *J. Appl. Meteor.,* **21,** 384–393.

Weinman, J. A., and Harshvardhan, 1982: Solar reflection from a regular array of horizontally finite clouds. *Appl. Opt.,* **21,** 2940–2944.